BIOCHEMISTRY
including biophysical chemistry & molecular biology

Article

pubs.acs.org/biochemistry

Ligand-Specific Structural Changes in the Vitamin D Receptor in Solution

Kiran K. Singarapu,[†,‡] Jinge Zhu,[‡] Marco Tonelli,[†,‡] Hongyu Rao,[‡] Fariba M. Assadi-Porter,[†,‡] William M. Westler,[†,‡] Hector F. DeLuca,[‡] and John L. Markley*[,†,‡]

[†]National Magnetic Resonance Facility at Madison and [‡]Department of Biochemistry, University of Wisconsin—Madison, 433 Babcock Drive, Madison, Wisconsin 53706, United States

ABSTRACT: Vitamin D receptor (VDR) is a member of the nuclear hormone receptor superfamily. When bound to a variety of vitamin D analogues, VDR manifests a wide diversity of physiological actions. The molecular mechanism by which different vitamin D analogues cause specific responses is not understood. The published crystallographic structures of the ligand binding domain of VDR (VDR-LBD) complexed with ligands that have differential biological activities have exhibited identical protein conformations. Here we report that rat VDR-LBD (rVDR-LBD) in solution exhibits differential chemical shifts when bound to three ligands that cause diverse responses: the natural hormone, 1,25-dihydroxyvitamin D_3 [1,25$(OH)_2D_3$], a potent agonist analogue, 2-methylene-19-nor-(20*S*)-1,25-dihydroxyvitamin D_3 [2MD], and an antagonist, 2-methylene-(22*E*)-(24*R*)-25-carbobutoxy-26,27-cyclo-22-dehydro-1α,24-dihydroxy-19-norvitamin D_3 [OU-72]. Ligand-specific chemical shifts mapped not only to residues at or near the binding pocket but also to residues remote from the ligand binding site. The complexes of rVDR-LBD with native hormone and the potent agonist 2MD exhibited chemical shift differences in signals from helix-12, which is part of the AF2 transactivation domain that appears to play a role in the selective recruitment of coactivators. By contrast, formation of the complex of rVDR-LBD with the antagonist OU-72 led to disappearance of signals from residues in helices-11 and -12. We present evidence that disorder in this region of the receptor in the antagonist complex prevents the attachment of coactivators.

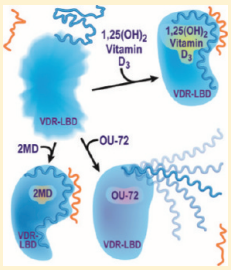

Vitamin D receptor (VDR) belongs to the type II class of nuclear hormone receptor superfamily, which comprises proteins that share a common structural architecture and are localized in the cell nucleus.[1] 1α,25-Dihydroxyvitamin D_3 [1,25$(OH)_2D_3$], the natural hormone that interacts with VDR, has been investigated in clinical treatment of divergent diseases including osteoporosis, cancers, autoimmune dysfunctions, cardiovascular diseases, and infections.[2−4] A recent study of the human genome sequence suggested that VDR binds to more than 2700 sites on the DNA and affects the expression levels of at least 229 gene products in response to vitamin D3.[5] Many analogues of 1,25$(OH)_2D_3$ have been prepared in an attempt to target specific actions of vitamin D.[6] VDR exhibits a wide diversity of physiological activities when bound to different vitamin D analogues; however, the molecular mechanism behind the ability of different vitamin D analogues to cause this diversity is yet to be elucidated.

Nuclear receptor ligand binding domains (LBDs) are known to undergo conformational changes upon binding of their physiological ligands, and this has been termed the "mouse trap" model.[7] Crystallographic and solution NMR studies of retinoid X receptor (RXR) α and peroxisome proliferator-activated receptor (PPAR) showed that they undergo conformational changes upon binding 9-*cis*-retinoic acid and rosiglitazone, respectively.[8,9] VDR contains two independent transactivation function (AF) domains: AF-1 located in the N-terminal region and AF-2 in the C-terminal or ligand binding region. The action of liganded VDR is mediated through heterodimerization with RXR and binding to vitamin D responsive elements found in the promoter and other target gene domains. This complex then binds coactivators and/or corepressors leading to activation/repression of target genes.[10] In the agonist-bound LBD structure, the AF-2 domain (consisting of helix-12) adopts a conformation (agonist conformation) allowing recruitment of coactivators, whereas in the antagonist bound LBD structure, the AF-2 domain adopts a different conformation (antagonist conformation) that prevents binding of coactivators, thereby preventing transcription.[11−16] It has been proposed that the differential biological activities of vitamin D analogues result from their stabilization of different VDR conformations. Nevertheless, no significant differences were observed in the conformation of the protein in crystal structures of complexes with ligands having very different biological activities.[17−19] Similar results were obtained in X-ray studies of the retinoic acid receptor, which exhibited the same protein conformation when bound to ligands differing in biological activity.[20,21] In both cases crystal packing forces apparently preserved the protein conformation and led to distortion of the ligand geometries.

Our hypothesis was that in solution, in the absence of crystal packing constraints, differences in the conformation of the VDR receptor when bound to diverse ligands should be observable by NMR spectroscopy. We selected a well-studied system, the vitamin D ligand binding domain construct of *Rattus norvegicus* (rVDR 116−423, Δ165−211) (rVDR-LBD) previously studied by X-ray crystallography,[17] and investigated

Received: October 27, 2011
Published: November 23, 2011

its conformation when bound to three ligands with different structures (Figure 1) and divergent biological effects:

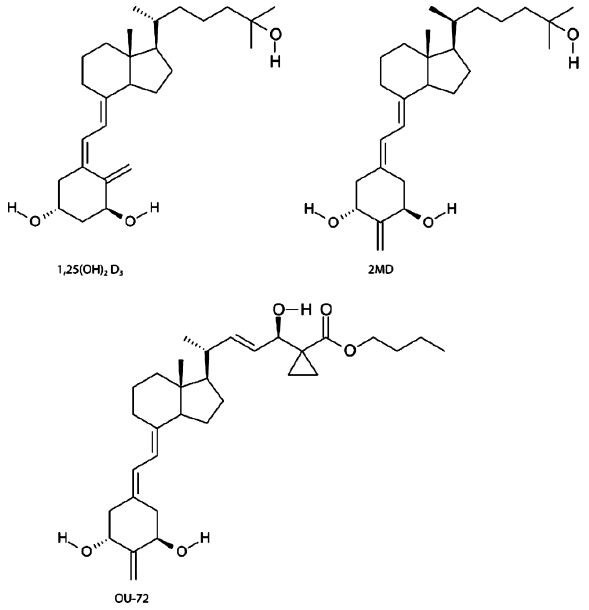

Figure 1. Chemical structures of VDR ligands that display divergent biological functions: $1,25(OH)_2D_3$ (natural hormone), 2MD (synthetic agonist analogue), OU-72 (synthetic antagonist analogue).

$1,25(OH)_2D_3$, the natural agonist; 2MD, a synthetic analogue that has been shown to increase bone Ca^{2+} resorption by 30-fold *in vivo* and by 2 orders of magnitude *in vitro*;[22] and OU-72, a potent antagonist that inhibits the transcription of $1,25(OH)_2D_3$-activated genes *in vitro*. Crystal structures solved for the complexes of rVDR-LBD bound to $1,25(OH)_2D_3$ (PDB id: 1RK3) and 2MD (PDB id: 1RJK) were found to have identical protein conformations,[17] and attempts to crystallize the complex containing OU-72 were unsuccessful. Here we report assigned NMR chemical shifts of rVDR-LBD when bound to these three ligands and document chemical shift differences that report on the differential influence of these ligands on the solution conformation of the protein.

MATERIALS AND METHODS

Production and Purification of [^{2}H,^{13}C,^{15}N]-rVDR-LBD. DNA coding for the ligand binding domain of the vitamin D receptor from *Rattus norvegicus* residues 116−423 with deletion of a 47 amino acid internal loop (165−211) (rVDR-LBD) was expressed as inclusion bodies in *Escherichia coli* BL21-CodonPlus(DE3)-RIPL cells grown at 37 °C in 200 mL of M9 medium in D_2O supplemented with [1,2,3,4,-5,6,6-^{2}H,U-^{13}C]-D-glucose (2 g/L) and either [^{2}H,^{13}C,^{15}N]-ISOGRO (5 g/L) for triple labeling or [^{2}H,^{15}N]-ISOGRO (5 g/L) for double labeling. The yield from the 200 mL culture was 4 mg of labeled VDR-LBD. The inclusion bodies were solubilized in 6 M guanidinium chloride and refolded by dialysis against a buffer containing 20 mM NaH_2PO_4−Na_2HPO_4 (pH 7.4), 50 mM KCl, and 2 mM DTT. The rVDR-LBD was purified to apparent homogeneity as analyzed by 12% SDS-PAGE. Aliquots of the pure labeled rVDR-LBD protein were incubated with desired ligands at 3−4-fold molar excess and concentrated to a final concentration of ∼0.5 mM in a buffer containing 20 mM NaH_2PO_4−Na_2HPO_4 (pH 7.4), 50 mM KCl, 5 mM DTT, 5X protease inhibitor (Roche), 0.05% NaN_3, and 7% D_2O. A 4-fold molar excess of the 13-residue peptide from DRIP205, which contains the LxxLL motif mimicking the coactivator, was added and incubated for 2 h at 4 °C. The protein concentration was determined by the Bradford method using bovine serum albumin as the standard. The ligand binding activity of LBD for all three ligands was confirmed with a competition assay as previously described.[23]

NMR Data Collection and Analysis. Unless otherwise noted, all NMR spectra were recorded on a Varian NMRS 900 MHz (^{1}H) spectrometer equipped with a cryogenic probe with the probe temperature adjusted to 25 °C. A series of two-dimensional (2D) and three-dimensional (3D) NMR spectra were collected using TROSY (transverse relaxation-optimized spectroscopy) based pulse sequence:[24] 3D-HNCO, 3D-HNCA, 3D-HN(CO)CA, 3D-HN(CA)CB, and ^{15}N-resolved 3D-^{1}H−^{1}H NOESY. The NMR data from these experiments were processed with NMRPipe[25] software and analyzed using the programs Xeasy[26] and SPARKY (T. D. Goddard and D. G. Kneller, SPARKY 3, University of California, San Francisco). Analysis of these spectra of rVDR-LBD complexed with $1,25(OH)_2D_3$ yielded sequence-specific assignments of the backbone, $^1H^{\beta}$, and $^{13}C^{\beta}$ resonances. Backbone resonance assignments were further confirmed by reference to ^{1}H−^{1}H NOE signals between the sequential amide ^{1}H resonances in the ^{15}N-resolved 3D ^{1}H−^{1}H NOESY spectrum. The backbone assignments were translated from the $1,25(OH)_2D_3$ complex to the other rVDR-LBD complexes by use of ^{15}N-resolved 3D-^{1}H−^{1}H NOESY spectra. A series of TROSY spectra of the rVDR-LBD complex with OU-72 were recorded as a function of temperature (25−45 at 5 °C intervals) on a Varian NMRS 600 MHz spectrometer to investigate the conformational dynamics of the C-terminus. The programs PECAN,[27] TALOS+,[28] and CSI[29] were used to predict secondary structural elements from the assigned $^1H^N$, ^{15}N, $^{13}C'$, $^{13}C^{\alpha}$, and $^{13}C^{\beta}$ chemical shifts. The chemical shift perturbations between the TROSY spectra for the different complexes were calculated using a weighted root-mean-square deviation formula:[30]

$$[0.5[\Delta\delta(^1H^N)^2 + (0.2\Delta\delta(^{15}N))^2]]^{1/2}$$

These magnitudes were used to color code the residues showing differences on the three-dimensional crystal structure of rVDR-LBD complexed to $1,25(OH)_2D_3$ (PDB id: 1RK3). PyMol[31] software was used for structure analysis and graphical display.

RESULTS

Stable isotope-labeled rVDR-LBD samples were produced and purified as recombinant protein in *Escherichia coli* cells. NMR spectra were recorded using TROSY-based pulse sequences on 900 or 600 MHz NMR spectrometers equipped with cryogenic probes regulated at the temperatures indicated.

The two-dimensional transverse relaxation optimized ^{1}H−^{15}N homonuclear single quantum correlation (TROSY-NHSQC) spectrum of ligand-free [U-^{2}H,U-^{15}N]-labeled rVDR-LBD displayed poor chemical shift dispersion and a large range of peak intensities, implying that the uncomplexed protein is structurally dynamic and undergoes order−disorder conformational exchange in solution (Figure 2, red spectrum). The addition of $1,25(OH)_2D_3$ to rVDR-LBD not only caused large changes in peak positions in the TROSY-NHSQC spectrum but also led to uniform signal intensities, indicating that the ligand bound protein adopts a single ordered conformation

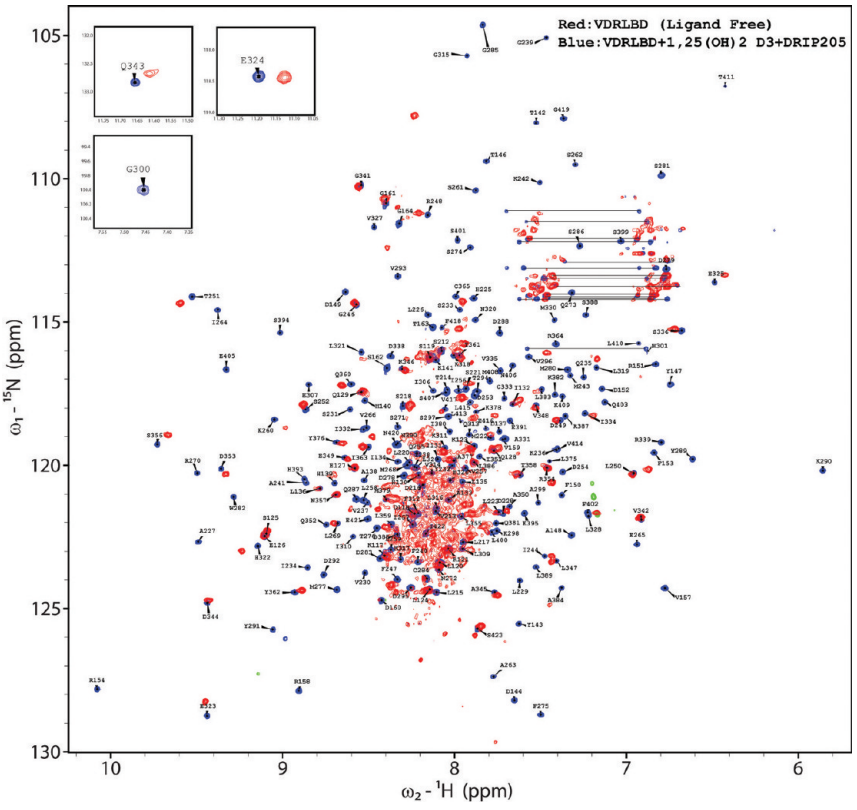

Figure 2. Superimposed TROSY NHSQC NMR spectra of (red) [U-^{2}H, U-^{15}N]-rVDR-LBD and (blue) [U-^{2}H, U-^{15}N]-rVDR-LBD complexed with 1,25$(OH)_2D_3$ in the presence of excess LxxLL peptide from DRIP205. Spectra were acquired at 25 °C on a Varian NMRS 900 MHz (^{1}H) NMR spectrometer equipped with a cryogenic probe. The amide resonances of the rVDR-LBD-1,25$(OH)_2D_3$ complex are labeled with sequence specific resonance assignments. Pairs of signals from the side chain amide resonances of Asn and Gln are connected by straight lines.

with uniform backbone dynamics in solution (Figure 2, blue spectrum). Similar ligand-induced conformational changes were observed for the 2MD (Figure 3) and OU-72 (Figure 4) complexes, although the signals from the AF-2 domain of the OU-72 complex were not observed, suggesting that they had been broadened beyond detection by conformational dynamics. We used TROSY-based triple-resonance experiments to determine sequence-specific assignments for 95% of the backbone resonances of [U-^{2}H,U-^{13}C,U-^{15}N]-rVDR-LBD complexed with 1,25$(OH)_2D_3$ and extended these assignments to the complexes with 2MD and OU-72. Assigned chemical shifts for rVDR-LBD complexed with 1,25$(OH)_2D_3$ and the LxxLL peptide have been deposited in BMRB[32] under accession number 17770. The assigned chemical shifts of the 1,25-$(OH)_2D_3$ complex were used to determine its secondary structural elements (Figure 5).

Comparison of the assigned TROSY-NHSQC spectra of the two agonist complexes (Figure 6a) revealed many small but significant chemical shift differences (Figure 7). Although these chemical shift differences were found globally, the major differences involved residues in the ligand binding pocket and reflected changes in the interfaces between the two ligands and the protein. In particular, the largest chemical shift differences mapped to residues in secondary structural elements, including helices-3, 5, 6, 7, 10, 11, 12 and the β-sheet and indicated that the largest structural changes are centered on residues V230 and I234 from helix-3. A similar comparison of the spectra of the 1,25$(OH)_2D_3$ complex with those of the OU-72 complex (Figure 6b) revealed a number of large chemical shift differences (indicated by arrows in the figure). In addition, peaks from several residues observed in the 1,25$(OH)_2D_3$ complex (circled in red) were absent in the OU-72 complex. The chemical shift differences between these two complexes are shown in Figure 8. We have mapped the chemical shift differences onto the X-ray structure of the ternary rVDR-LBD-1,25$(OH)_2D_3$-LxxLL peptide complex (Figure 9).

DRIP205 is a known coactivator of VDR, and a helical fragment of this protein containing the consensus sequence LxxLL (KNHPMLMNLLKDN-NH_2) has been shown to be responsible for transactivation of VDR *in vivo* as well as *in vitro*.[33] Binding of this LxxLL-containing peptide to [U-^{2}H,U-^{15}N]-rVDR-LBD complexed with 1,25$(OH)_2D_3$ resulted in small but significant chemical shift changes in the TROSY-NHSQC spectrum, confirming that LxxLL binds to rVDR-LBD in solution (Figure 10a). Specifically, the residues in the surface patch corresponding to helix-3, helix-4, and helix-12 involving the amide resonances of residues 239−246, 251−263, and 410−418 showed significant chemical shift changes upon binding the peptide, with residues K242 and E416 displaying the largest effects. These results support the hypothesis that in solution the coactivator consensus peptide and presumably coactivator proteins interact with the surface of rVDR-LBD near the AF-2 domain. We observed a similar pattern of TROSY-NHSQC chemical shift changes upon adding the LxxLL-containing peptide to [U-^{2}H,U-^{15}N]-rVDR-LBD complexed with 2MD. By contrast, the TROSY-NHSQC spectrum of [U-^{2}H,U-^{15}N]-rVDR-LBD complexed with the

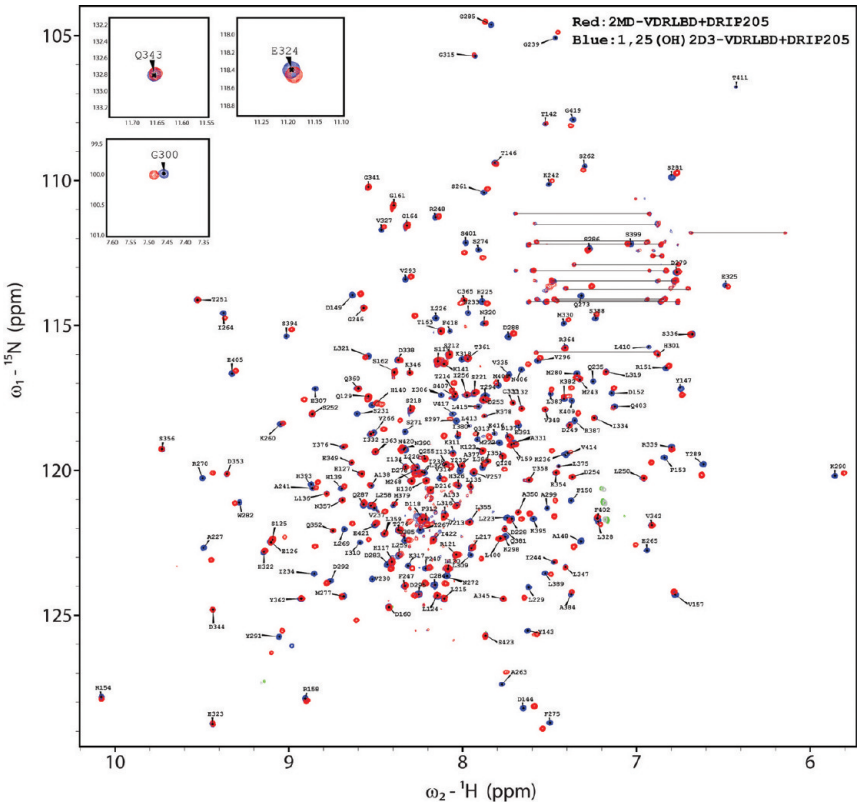

Figure 3. Superposed TROSY NHSQC NMR spectra of [U-^{2}H, U-^{15}N]-rVDR-LBD (red) complexed with 2MD and (blue) complexed with 1,25$(OH)_2D_3$. Both samples contained excess LxxLL peptide from DRIP205. Data were collected at 25 °C on a Varian NMRS 900 MHz (^{1}H) NMR spectrometer equipped with a cryogenic probe. The amide resonances of rVDR-LBD complexed with 1,25$(OH)_2D_3$ are labeled with sequence specific resonance assignments. Pairs of signals from the side-chain amide resonances of Asn and Gln are connected by straight lines.

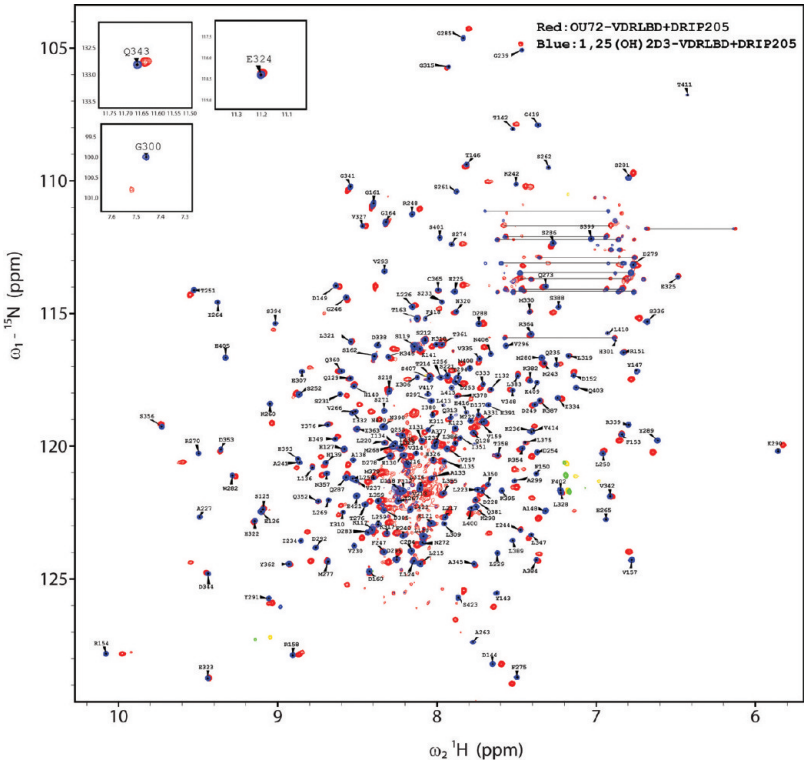

Figure 4. Superposed TROSY NHSQC NMR spectra of [U-^{2}H, U-^{15}N]-rVDR-LBD (red) complexed with OU-72 and (blue) complexed with 1,25$(OH)_2D_3$. Both samples contained excess LxxLL peptide from DRIP205. Data were collected at 25 °C on a Varian NMRS 900 MHz (^{1}H) NMR spectrometer equipped with a cryogenic probe. The amide resonances of rVDR-LBD complexed with 1,25$(OH)_2D_3$ are labeled with sequence specific resonance assignments. Pairs of signals from the side chain amide resonances of Asn and Gln are connected by straight lines.

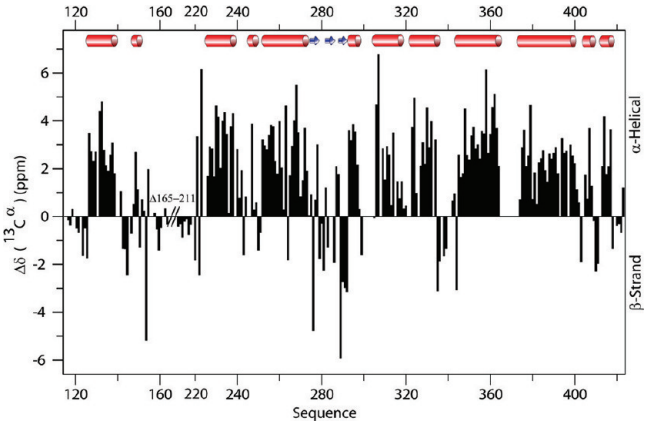

Figure 5. Secondary structural elements determined from chemical shifts and secondary $^{13}C^{\alpha}$ chemical shifts (experimental minus random coil) for rVDR-LBD complexed with $1,25(OH)_2D_3$ and the LxxLL peptide from DRIP205. Secondary structural elements determined from the assigned chemical shifts are represented by red cylinders for α-helices and blue arrows for β-strands. The secondary $^{13}C^{\alpha}$ chemical shifts were determined by the CYANA[35] program.

antagonist OU-72, failed to exhibit chemical shift changes upon addition of the LxxLL-containing peptide (Figure 10b).

DISCUSSION

In the crystal structures of rVDR-LBD complexed with $1,25(OH)_2D_3$ (PDB id: 1RK3; resolution: 2.2 Å) and 2MD (PDB id: 1RJK; resolution: 1.99 Å), the protein conformations were identical. We have shown here by NMR spectroscopy that in solution the same complexes display significant differences in the chemical shifts of the amide resonances, indicating differences in structure (Figure 9).

Amide chemical shifts are sensitive to the electronic environment in the native fold of the protein, and their changes arise primarily from differences in H-bonding strengths, patterns, or alteration of backbone torsion angles. It has been shown that the chemical shifts of the amide proton ($^1H_i^N$) and nitrogen ($^{15}N_i$) are highly correlated with ϕ_i and ψ_{i-1} torsion angles.[34] The lower than expected number of signals in the TROSY-NHSQC NMR spectrum of ligand-free rVDR-LBD (Figure 2), along with their lack of dispersion and large range of peak intensities, indicates that a significant portion of the protein undergoes conformational dynamics. Upon formation of the rVDR-LBD-$1,25(OH)_2D_3$ binary complex, the TROSY-NHSQC NMR spectrum became dispersed, and signals with uniform intensities were observed for nearly all residues. (Figure 2). These differences suggest that the conformation flexibility observed for apo-rVDR-LBD is quenched upon binding to $1,25(OH)_2D_3$. Nearly complete sequence-specific backbone resonance assignments were obtained for the rVDR-LBD complex with $1,25(OH)_2D_3$ by analysis of TROSY-based triple-resonance experiments (Figure 2). The binary complexes of rVDR-LBD with 2MD (Figure 3) and OU-72 (Figure 4) also yielded well-dispersed spectra, indicating that the ligand-bound protein is well structured. Spectra of the $1,25(OH)_2D_3$ and 2MD binary complexes (Figure 3) and the $1,25(OH)_2D_3$ and OU-72 binary complexes (Figure 4) exhibited widespread

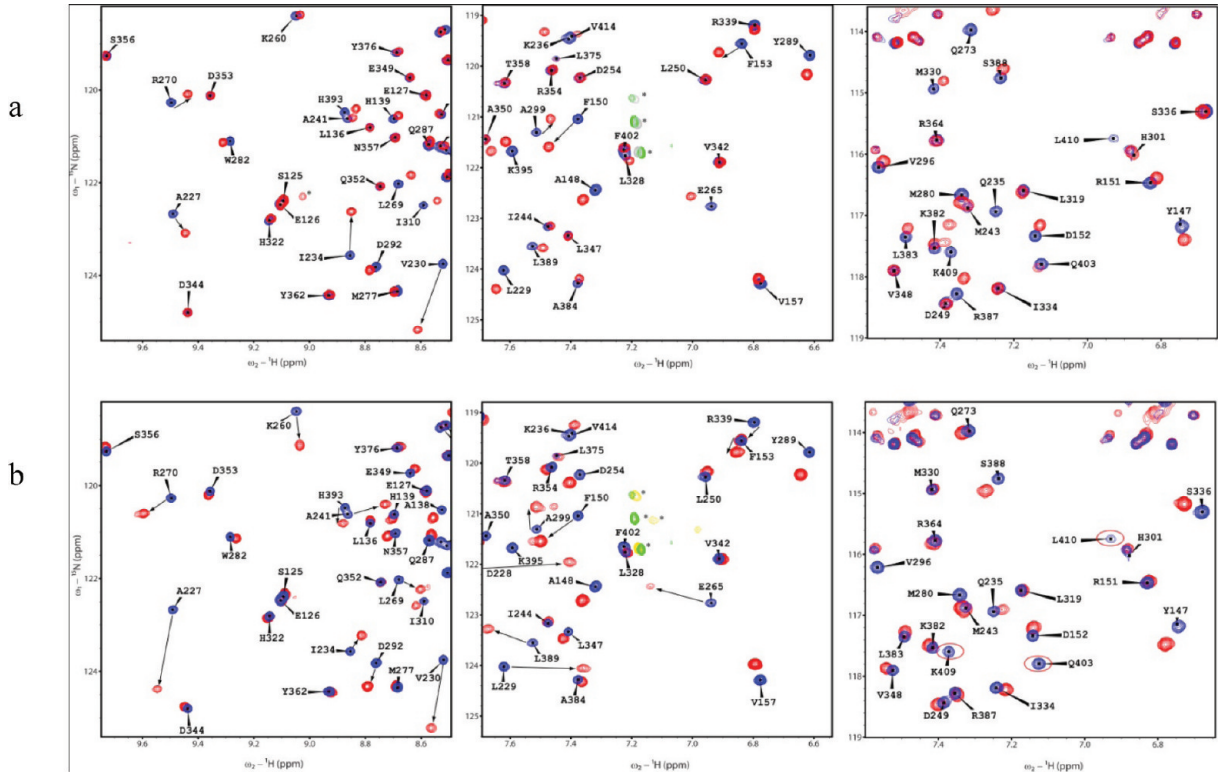

Figure 6. Superposed TROSY NHSQC NMR spectra: (a) [U-^{2}H,U-^{15}N]-rVDR-LBD complexed with (blue) $1,25(OH)_2D_3$ and (red) 2MD. (b) [U-^{2}H,U-^{15}N]-rVDR-LBD complexed with (blue) $1,25(OH)_2D_3$ and (red) OU-72. Excess LxxLL peptide from DRIP205 was present in all samples. Data were collected at 25 °C on a Varian NMRS 900 MHz (^{1}H) NMR spectrometer equipped with a cryogenic probe. In each panel, the amide resonances of rVDR-LBD complexed with $1,25(OH)_2D_3$ are labeled with sequence specific resonance assignments. Circled in red are the peaks in the $1,25(OH)_2D_3$ complex whose corresponding peaks in the OU-72 complex were not observed. Peaks colored green and yellow are from unassigned signals aliased into this spectral region.

dx.doi.org/10.1021/bi201637p | *Biochemistry* 2011, 50, 11025–11033

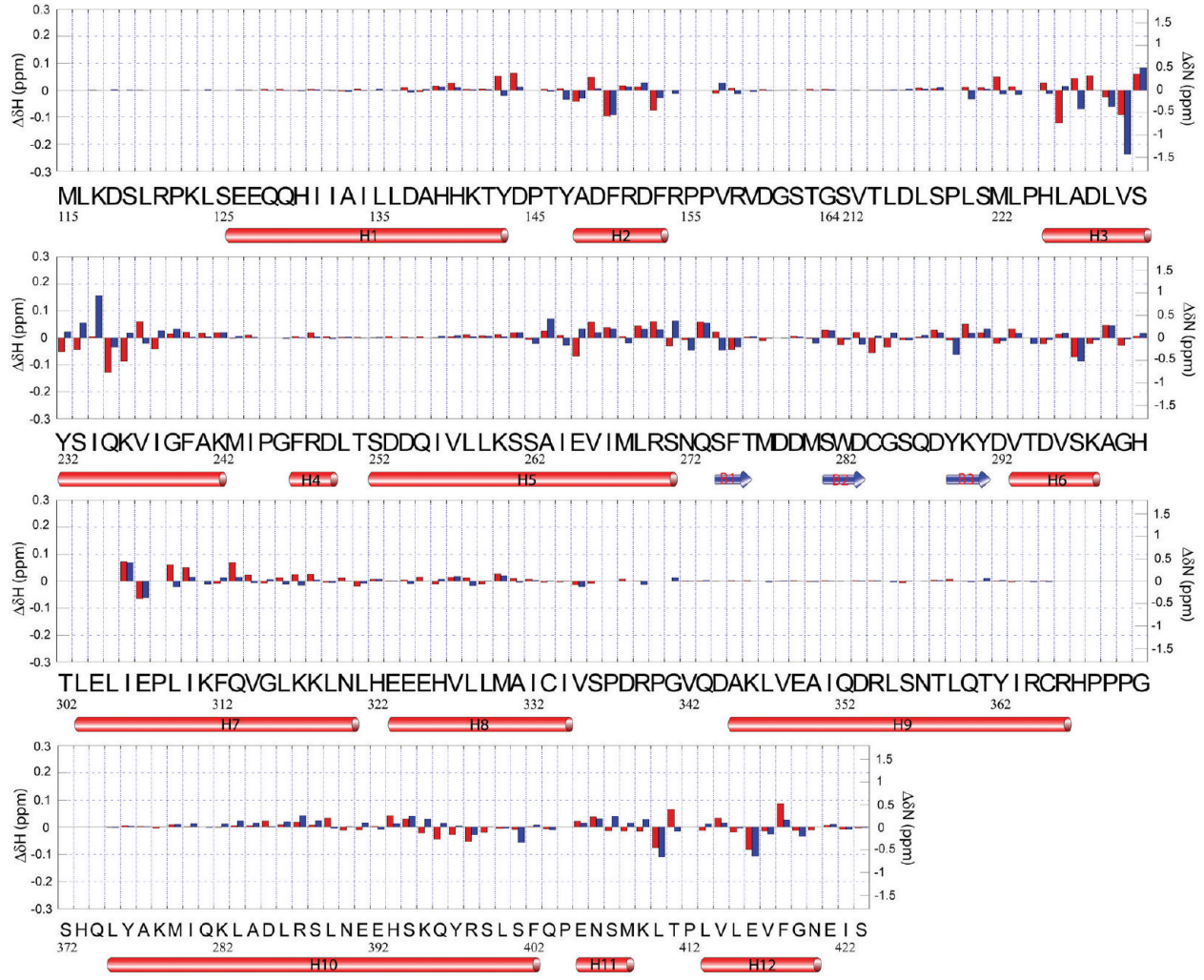

Figure 7. Differences in the amide proton ($\Delta\delta$H, red) and amide nitrogen ($\Delta\delta$N, blue) chemical shifts of rVDR-LBD-(LxxLL-containing peptide) complexed with 1,25$(OH)_2D_3$ and 2MD. The amide proton and amide nitrogen shifts are scaled by their respective chemical shift ranges. Secondary structural elements determined from the assigned chemical shifts of the rVDR-LBD-(LxxLL-containing peptide)-1,25$(OH)_2D_3$ ternary complex are represented by red cylinders for α-helices and blue arrows for β-strands.

chemical shift differences. Those from residues in or near the ligand binding pocket could, in principle, only reflect differential interactions with the ligands, but those from residues remote from the binding pocket are indicative of ligand-induced conformational changes. Secondary structural elements predicted by the PECAN,[27] TALOS+,[28] and CSI[29] programs for rVDR-LBD in the 1,25$(OH)_2D_3$ complex were in agreement with one another; the positions of the 12 α-helices and 3 short β-strands predicted by these programs are compared in Figure 5 with the $^{13}C^{\alpha}$ secondary chemical shifts calculated by CYANA.[35]

Addition of the LxxLL-containing peptide corresponding to the helical fragment from the coactivator DRIP205 to the rVDR-LBD-1,25$(OH)_2D_3$ complex resulted in small but significant chemical shift changes for amide peaks in the TROSY-NHSQC spectrum, confirming that the peptide binds to this complex (Figure 10a). By contrast, signals from the rVDR-LBD-OU-72 complex did not show appreciable chemical shift changes upon addition of the LxxLL peptide, suggesting that the peptide does not bind under these conditions (Figure 10b). The rVDR-LBD-OU-72 complex may lack a stable binding surface for the peptide because of the conformational dynamics observed in the AF-2 domain.

The molecular mechanism of action of antagonist-bound nuclear receptors is significantly different from that of the agonist-bound receptors. In the estrogen receptor (ERα), it has been shown that binding of the antagonists raloxifen or tamoxifen causes movement of the ERα AF-2 domain preventing coactivator binding.[15,16] This suggests that the activation and inhibition of gene transcription utilize different molecular mechanisms. In the case of VDR, OU-72 has been identified as a potential antagonist that inhibits the transcription of several gene targets. rVDR-LBD complexed with OU-72 exhibited a high quality TROSY-NHSQC spectrum with significant and global spectral (structural) differences from that of the rVDR-LBD complex with 1,25$(OH)_2D_3$ (Figure 4). Apart from changes in the chemical shifts of residues in the ligand binding site, the most striking difference was the absence of amide peaks corresponding to residues 395−421 in the spectrum of the OU-72 complex (Figure 6). An explanation for the absence of these resonances (corresponding to residues colored pink in Figure 9) is that residues in helices-11 and -12 are structurally dynamic and visit two or more conformations at exchange rates on the intermediate NMR time scale where signals are broadened beyond detection. This result, which indicates that the AF2

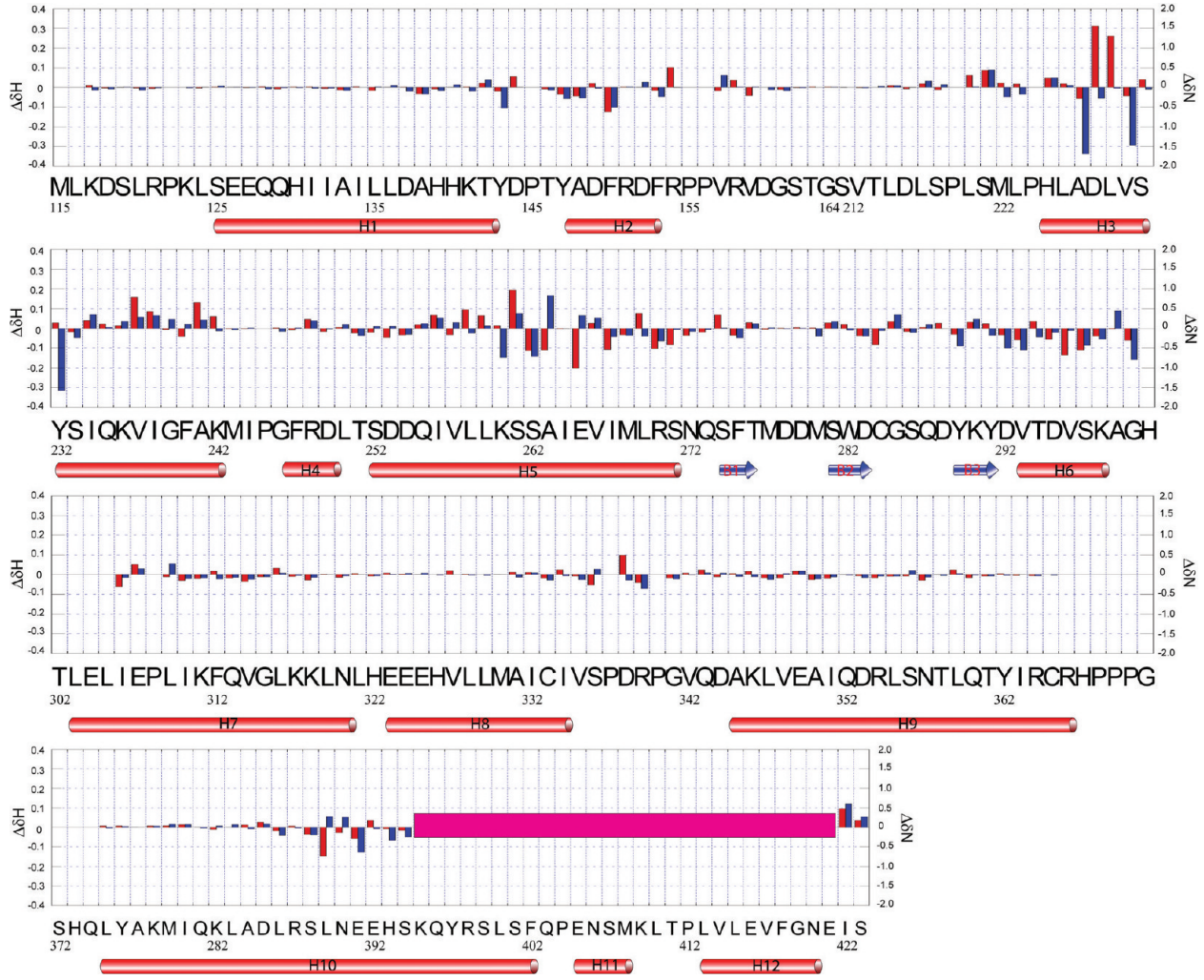

Figure 8. Differences in the amide proton ($\Delta\delta$H, red) and amide nitrogen ($\Delta\delta$N, blue) chemical shifts of rVDR-LBD complexed with 1,25$(OH)_2D_3$ and OU-72. The amide proton and amide nitrogen shifts are scaled by their respective chemical shift ranges. Secondary structural elements are represented by red cylinders for α-helices and blue arrows for β-strands. In the OU-72 complex, signals from residues 395−421 (indicated by the pink bar) were not observed in the 900 MHz (^{1}H) TROSY-HSQC spectrum collected at 25 °C.

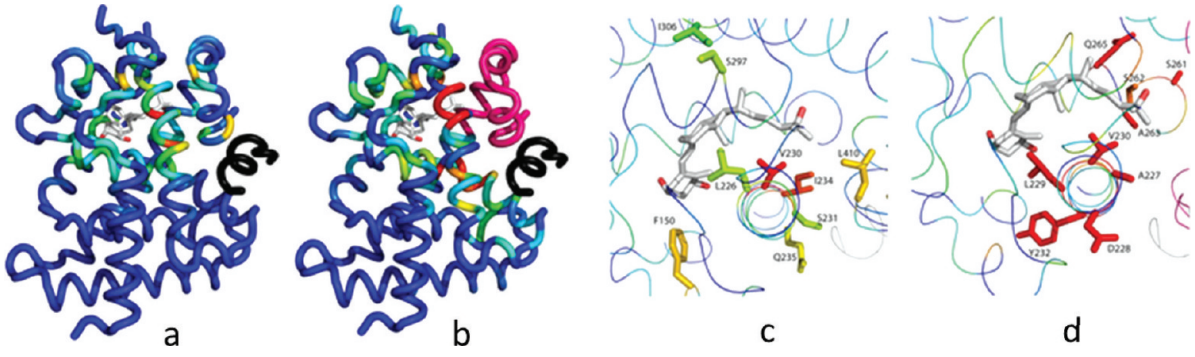

Figure 9. (panels a and b) Crystal structure of the rVDR-LBD-(LxxLL-containing peptide)-1,25$(OH)_2D_3$ ternary complex (PDB 1RK3) color coded by the chemical shift differences between: (a) the ternary complexes with 1,25$(OH)_2D_3$ and 2MD (both agonists) and (b) the ternary complexes with 1,25$(OH)_2D_3$ (natural agonist) and OU-72 (an antagonist). Weighted backbone ^{1}H−^{15}N chemical shift differences are color-coded from red for residues with large shifts to blue for residues with small or no shift. The coactivator peptide (LxxLL) is displayed in black, and the ligand (1,25$(OH)_2D_3$) is modeled by gray sticks. The pink backbone in (b) indicates residues of rVDR-LBD whose amide resonances were not observed in the 900 MHz TROSY-NHSQC spectrum of the OU-72 ternary complex. (panels c and d) Ligand binding site of the rVDR-LBD-(LxxLL-containing peptide)-1,25$(OH)_2D_3$ ternary complex (PDB 1RK3) showing residues color coded by the magnitude of their chemical shift differences between (c) the ternary complexes with 1,25$(OH)_2D_3$ and 2MD (both agonists) and (d) the ternary complexes with 1,25$(OH)_2D_3$ (natural agonist) and OU-72 (an antagonist). The side chains of the 10 residues showing the largest weighted backbone ^{1}H−^{15}N chemical shift differences are displayed as sticks.

dx.doi.org/10.1021/bi201637p | *Biochemistry* 2011, 50, 11025−11033

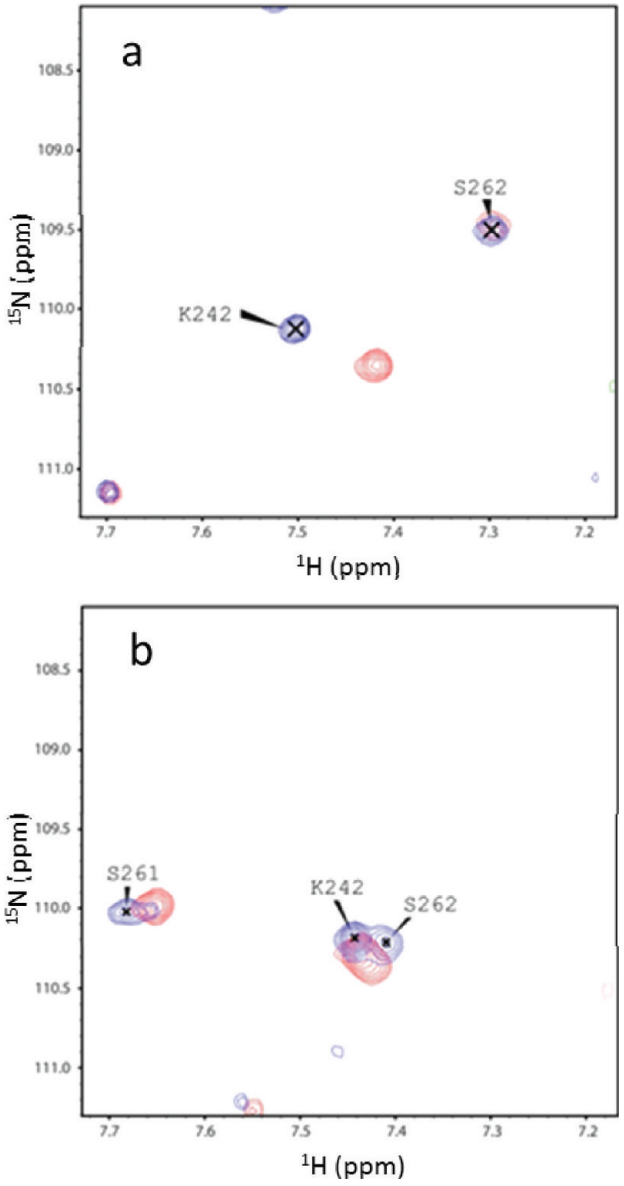

Figure 10. Comparison of selected regions of TROSY NHSQC NMR spectra of (a) the rVDR-LBD-1,25$(OH)_2D_3$ complex (blue) without and (red) with added LxxLL peptide and (b) the rVDR-LBD-OU-72 complex (blue) without and (red) with added LxxLL peptide. The protein was [U-^{2}H,U-^{15}N]-labeled. Data were collected at 25 °C on a Varian NMRS 900 MHz (^{1}H) NMR spectrometer equipped with a cryogenic probe.

domain in the antagonist bound complex does not adopt a single conformation in solution, may explain why attempts to crystallize the rVDR-LBD-OU-72 complex have failed. Support for the dynamic model of the rVDR-LBD complex with OU-72 also comes from the finding (Figure 11) that some of the peaks missing in data collected at 25 °C and 21.1 T (900 MHz for ^{1}H) appear in spectra collected at a higher temperature 40 °C and lower magnetic field strength 14.1 T (600 MHz for ^{1}H), conditions that shift the NMR time scale toward the fast exchange limit where peaks from exchanging groups become sharper.

The finding that rVDR-LBD complexes with ligands and coactivators causing diverse physiological responses exhibit distinct spectral signatures demonstrates that NMR spectroscopy offers a powerful platform for the systematic study of this

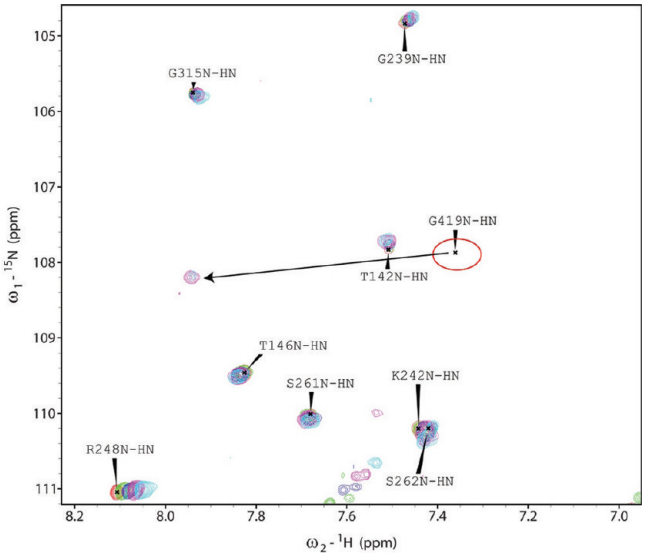

Figure 11. Superposition of 600 MHz (^{1}H) TROSY NHSQC NMR spectra of the [^{2}H,^{15}N]-rVDR-LBD-OU-72 complex in the presence of the LxxLL peptide from DRIP205 collected at 5 °C intervals between 25 and 45 °C. Color coding: red, 25 °C; green, 30 °C; blue, 35 °C; magenta, 40 °C; and cyan, 45 °C. Peaks denoted by "×" correspond to assignments for the rVDR-LBD-1,25$(OH)_2D_3$ complex. The arrow points to the peaks detected at 40 and 45 °C assigned to G419; these peaks were not observed in the 900 MHz spectrum collected at 25 °C.

important member of the nuclear hormone receptor superfamily. Studies are underway aimed at determining the solution structures of the complexes described here.

AUTHOR INFORMATION

Corresponding Author

*Tel: 608-263-9349; e-mail: markley@nmrfam.wisc.edu.

Funding

This work was supported by funding from Wisconsin Alumni Research Foundation to H.F.D. and grants from the U.S. National Institutes of Health to J.L.M. in support of the National Magnetic Resonance Facility at Madison (P41 RR0231 and P41 RR02301-25S1) and to F.M.A.-P. (R01 DC009018).

DEDICATION

This paper is dedicated to the memory of Norma Marchesini.

REFERENCES

(1) Mangelsdorf, D. J., Thummel, C., Beato, M., Herrlich, P., Schutz, G., Umesono, K., Blumberg, B., Kastner, P., Mark, M., Chambon, P., and Evans, R. M. (1995) The nuclear receptor superfamily: the second decade. *Cell 83*, 835−839.

(2) DeLuca, H. F. (2008) Evolution of our understanding of vitamin D. *Nutr. Rev. 66*, S73−S87.

(3) Holick, M. F. (2008) The vitamin D deficiency pandemic and consequences for non-skeletal health: Mechanism of action. *Mol. Aspects Med. 29*, 361−368.

(4) Bikle, D. (2009) Nonclassic Actions of Vitamin D. *J. Clin. Endocrinol. Metab. 94*, 26−34.

(5) Ramagopalan, S. V., Heger, A., Berlanga, A. J., Maugeri, N. J., Lincoln, M. R., Burrell, A., Handunnetthi, L., Handel, A. E., Disanto, G., Orton, S. M., Watson, C. T., Morahan, J. M., Giovannoni, G., Ponting, C. P., Ebers, G. C., and Knight, J. C. (2010) A ChIP-seq defined genome-wide map of vitamin D receptor binding: Associations with disease and evolution. *Genome Res. 20*, 1352−1360.

(6) Brown, A. J., and Slatopolsky, E. (2008) Vitamin D analogs: Therapeutic applications and mechanisms for selectivity. *Mol. Aspects Med. 29*, 433−452.
(7) Wurtz, J. M., Bourguet, W., Renaud, J. P., Vivat, V., Chambon, P., Moras, D., and Gronemeyer, H. (1996) A canonical structure for the ligand-binding domain of nuclear receptors. *Nat. Struct. Biol. 3*, 87−94.
(8) Lu, J. Y., Cistola, D. P., and Li, E. (2006) Analysis of ligand binding and protein dynamics of human retinoid X receptor alpha ligand-binding domain by nuclear magnetic resonance. *Biochemistry 45*, 1629−1639.
(9) Johnson, B. A., Wilson, E. M., Li, Y., Moller, D. E., Smith, R. G., and Zhou, G. C. (2000) Ligand-induced stabilization of PPAR gamma monitored by NMR spectroscopy: Implications for nuclear receptor activation. *J. Mol. Biol. 298*, 187−194.
(10) MacDonald, P., and Dowd, D. R. (2011) Vitamin D, in *Vitamin D* (Feldman, D., Pike, J. W., and Adams, J. S., Eds.) 3rd ed., pp 193−209, Elsevier, London.
(11) Nolte, R. T., Wisely, G. B., Westin, S., Cobb, J. E., Lambert, M. H., Kurokawa, R., Rosenfeld, M. G., Willson, T. M., Glass, C. K., and Milburn, M. V. (1998) Ligand binding and co-activator assembly of the peroxisome proliferator-activated receptor-gamma. *Nature 395*, 137−143.
(12) Bourguet, W., Ruff, M., Chambon, P., Gronemeyer, H., and Moras, D. (1995) Crystal Structure of the Ligand-Binding Domain of the Human Nuclear Receptor RXR-alpha. *Nature 375*, 377−382.
(13) Huang, P. X., Chandra, V., and Rastinejad, F. (2010) Structural Overview of the Nuclear Receptor Superfamily: Insights into Physiology and Therapeutics. *Annu. Rev. Physiol. 72*, 247−272.
(14) Moras, D., and Gronemeyer, H. (1998) The nuclear receptor ligand-binding domain: structure and function. *Curr. Opin. Cell Biol. 10*, 384−391.
(15) Shiau, A. K., Barstad, D., Loria, P. M., Cheng, L., Kushner, P. J., Agard, D. A., and Greene, G. L. (1998) The structural basis of estrogen receptor/coactivator recognition and the antagonism of this interaction by tamoxifen. *Cell 95*, 927−937.
(16) Brzozowski, A. M., Pike, A. C., Dauter, Z., Hubbard, R. E., Bonn, T., Engstrom, O., Ohman, L., Greene, G. L., Gustafsson, J. A., and Carlquist, M. (1997) Molecular basis of agonism and antagonism in the oestrogen receptor. *Nature 389*, 753−758.
(17) Vanhooke, J. L., Benning, M. M., Bauer, C. B., Pike, J. W., and DeLuca, H. F. (2004) Molecular structure of the rat vitamin D receptor ligand binding domain complexed with 2-carbon-substituted vitamin D-3 hormone analogues and a LXXLL-containing coactivator peptide. *Biochemistry 43*, 4101−4110.
(18) Vanhooke, J. L., Tadi, B. P., Benning, M. M., Plum, L. A., and DeLuca, H. F. (2007) New analogs of 2-methylene-19-nor-(20S)-1,25-dihydroxyvitamin D-3 with conformationally restricted side chains: Evaluation of biological activity and structural determination of VDR-bound conformations. *Arch. Biochem. Biophys. 460*, 161−165.
(19) Tocchini-Valentini, G., Rochel, N., Wurtz, J. M., Mitschler, A., and Moras, D. (2001) Crystal structures of the vitamin D receptor complexed to superagonist 20-epi ligands. *Proc. Natl. Acad. Sci. U. S. A. 98*, 5491−5496.
(20) Klaholz, B. P., Mitschler, A., Belema, M., Zusi, C., and Moras, D. (2000) Enantiomer discrimination illustrated by high-resolution crystal structures of the human nuclear receptor hRAR gamma. *Proc. Natl. Acad. Sci. U. S. A. 97*, 6322−6327.
(21) Klaholz, B. P., Renaud, J. P., Mitschler, A., Zusi, C., Chambon, P., Gronemeyer, H., and Moras, D. (1998) Conformational adaptation of agonists to the human nuclear receptor RAR gamma. *Nat. Struct. Biol. 5*, 199−202.
(22) Shevde, N. K., Plum, L. A., Clagett-Dame, M., Yamamoto, H., Pike, J. W., and DeLuca, H. F. (2002) A potent analog of 1 alpha,25-dihydroxyvitamin D-3 selectively induces bone formation. *Proc. Natl. Acad. Sci. U. S. A. 99*, 13487−13491.
(23) Glebocka, A., Sicinski, R. R., Plum, L. A., Clagett-Dame, M., and DeLuca, H. F. (2006) New 2-alkylidene 1 alpha,25-dihydroxy-19-norvitamin D-3 analogues of high intestinal activity: Synthesis and biological evaluation of 2-(3 '-alkoxypropylidene) and 2-(3-hydroxypropylidene) derivatives. *J. Med. Chem. 49*, 2909−2920.
(24) Pellecchia, M., Sebbel, P., Hermanns, U., Wuthrich, K., and Glockshuber, R. (1999) Pilus chaperone FimC-adhesin FimH interactions mapped by TROSY- NMR. *Nat. Struct. Biol. 6*, 336−339.
(25) Delaglio, F., Grzesiek, S., Vuister, G. W., Zhu, G., Pfeifer, J., and Bax, A. (1995) NMRPIPE - A Multidimensional Spectral Processing System Based on UNIX Pipes. *J. Biomol. NMR 6*, 277−293.
(26) Bartels, C., Xia, T. H., Billeter, M., Güntert, P., and Wüthrich, K. (1995) The Program XEASY for Computer-Supported NMR Spectral-Analysis of Biological Macromolecules. *J. Biomol. NMR 5*, 1−10.
(27) Eghbalnia, H. R., Wang, L., Bahrami, A., Assadi, A., and Markley, J. L. (2005) Protein energetic conformational analysis from NMR chemical shifts (PECAN) and its use in determining secondary structural elements. *J. Biomol. NMR 32*, 71−81.
(28) Shen, Y., Delaglio, F., Cornilescu, G., and Bax, A. (2009) TALOS+: a hybrid method for predicting protein backbone torsion angles from NMR chemical shifts. *J. Biomol. NMR 44*, 213−223.
(29) Wishart, D. S., and Sykes, B. D. (1994) The ^{13}C Chemical Shift Index: A Simple Method for the Identification of Protein Secondary Structure Using ^{13}C Chemical Shifts. *J. Biomol. NMR 4*, 171−180.
(30) Farmer, B. T. II (1996) Localizing The NADP + Binding Site on the Murb Enzyme by NMR. *Nat. Struct. Biol. 3*, 995−997.
(31) DeLano, W. L., and Lam, J. W. (2005) PyMOL: A communications tool for computational models. *Abstr. Pap. Am. Chem. Soc. 230*, U1371−U1372.
(32) Ulrich, E. L., Akutsu, H., Doreleijers, J. F., Harano, Y., Ioannidis, Y. E., Lin, J., Livny, M., Mading, S., Maziuk, D., Miller, Z., Nakatani, E., Schulte, C. F., Tolmie, D. E., Kent Wenger, R., Yao, H., and Markley, J. L. (2008) BioMagResBank. *Nucleic Acids Res. 36*, D402−408.
(33) Heery, D. M., Kalkhoven, E., Hoare, S., and Parker, M. G. (1997) A signature motif in transcriptional co-activators mediates binding to nuclear receptor. *Nature 387*, 733−736.
(34) Le, H., and Oldfield, E. (1994) Correlation between 15N NMR chemical shifts in proteins and secondary structure. *J. Biomol. NMR 4*, 341−348.
(35) Güntert, P. (2004) Automated NMR structure calculation with CYANA. *Methods Mol. Biol. 278*, 353−378.

NOTE ADDED AFTER ASAP PUBLICATION

After this paper was published online December 5, 2011, corrections were made to Figures 2, 3, 4, 7, and 8. The revised version was published December 20, 2011.